Steps toward pre-clinical iPSC-derived kindey organoids

Wiersma, L.E.

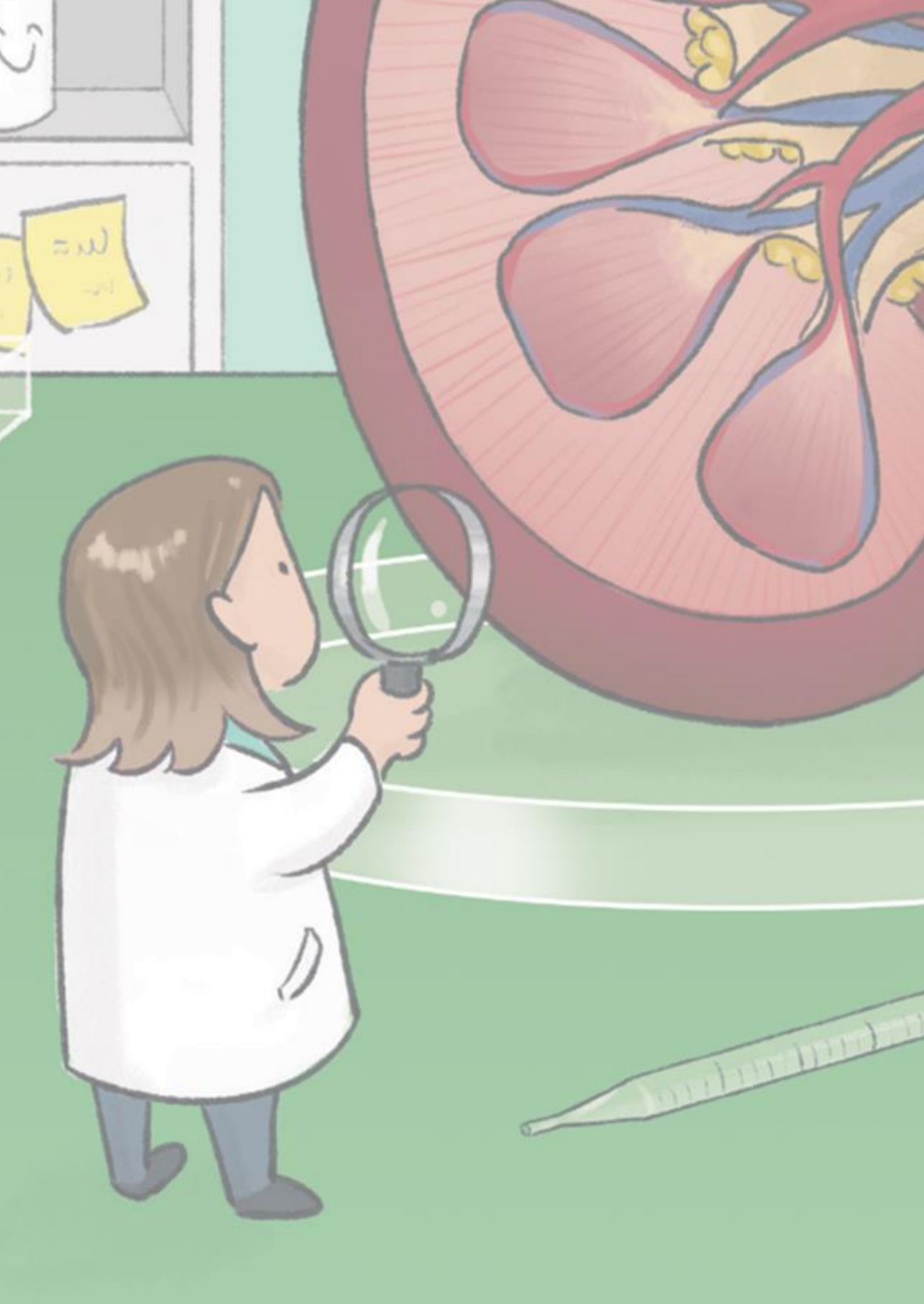

Chapter 3

Assessment of hiPSC derived kidney organoids from cryopreserved progenitors using MALDI-MSI

Loes E. Wiersma[1,2,3], Gangqi Wang[1,2,3], Ton J. Rabelink[1,2,3], Cathelijne W. van den Berg[1,2,3]

[1] Department of Internal Medicine - Nephrology, Leiden University Medical Center, Albinusdreef 2, 2333 ZA Leiden, The Netherlands
[2] Einthoven Laboratory of Vascular and Regenerative Medicine, Leiden University Medical Center, Albinusdreef 2, 2333 ZA Leiden, the Netherlands
[3] The Novo Nordisk Foundation Center for Stem Cell Medicine (reNEW), Leiden University Medical Center (LUMC), Albinusdreef 2, 2333 ZA Leiden, the Netherlands

Heliyon 12 (2026) e44067

Abstract

Induced pluripotent stem cell (iPSC) derived kidney organoids are three-dimensional aggregates that self-organize in a permissive environment, and exhibit structural similarities to the adult kidney. The potential application of these tissues in regenerative medicine as a clinical therapy is currently investigated. Before such therapies can be realized, comprehensive assessment of the cell types present in kidney organoids is required. We recently proposed MALDI-MSI (Matrix-Assisted Laser Desorption Ionization - Mass spectrometry imaging) as a technology for evaluating cellular composition of intact tissue samples. This approach removes the need for tissue dissociation, thereby preserving architecture and maintaining specific cell populations. Consequently, this technology could be explored for in depth characterization of cell composition in cultured kidney organoids. In this study, we cryopreserved iPSC-derived kidney progenitors at day 7 of differentiation and demonstrate that their differentiation could be successfully resumed after thawing. We then applied MALDI-MSI to assess quality of the kidney organoids and evaluated the cell types present by analyzing their lipid profiles. In parallel, we used immunohistochemistry to identify specific cell types, including glomeruli as well as proximal and distal tubular structures. Importantly, lipidomics profiling using MALDI-MSI provided a more comprehensive cellular overview of tissue composition, allowing us to directly compare cryopreserved and non-cryopreserved kidney organoids. In conclusion, we suggest MALDI-MSI as a platform that can be used for in depth cell type analysis of kidney organoid cultures.

Keywords: iPSC-derived kidney organoids, cryopreservation, regenerative medicine, MALDI-MSI, transplantation

Highlights

- PSC-derived kidney organoid progenitors continue differentiation upon cryopreservation
- MALDI-MSI provides a detailed molecular profile of kidney organoids
- MALDI-MSI could serve as a platform for qualitative assessment of complex tissues

Glossary / Abbreviations

cKOR	cryopreserved kidney organoid
CAR	chimeric antigen receptor
DMEM	Dulbecco's Modified Eagle Medium
E8	Essential 8
EDTA	Ethylenediaminetetraacetic acid
iPSCs	Induced pluripotent stem cells
KOR	Kidney organoid
LTL	Lotus Tetragonolobus Lectin
MALDI	Matrix-assisted laser desorption ionization
MSI	Mass spectrometry imaging
PBS	phosphate-buffered saline
PFA	Paraformaldehyde
PFHMII	Protein-Free Hybridoma Medium-II
rhFGF9	recombinant human Fibroblast growth factor-9
SLC12A1	Solute Carrier Family 12 Member 1
TCR	T-cell receptor
TIC	total ion count
TOF	Time-Of-Flight
UMAP	Uniform manifold approximation and projection

Introduction

Kidney organoids recapitulate key features of human renal development. In the past decade, multiple protocols to differentiate (induced) pluripotent stem cells ((i)PSCs) into kidney organoids have been developed [1,2]. These organoids have been proposed as potential future replacement therapies for patients with reduced kidney function, and are widely used to study human (kidney) development [3], perform human kidney disease modeling, and screen candidate drugs.

Technologies for generating kidney organoids (KORs) have advanced substantially, and methods for upscaling have been described both for the initial phase of the differentiation as well as for the end product as nephron sheets or patches [4,5] or suspension culture [6,7]. [6,7]. For clinical manufacturing PSCs and PSC-derived products, it is essential to establish validated master cell banks and adhere to Good Manufacturing Practice (GMP)-compliant procedures [8]. As such, further characterization and quality assessment of PSCs and/or PSC-derived tissues after scale up or following cryopreservation is critical. While brightfield and immunofluorescence imaging have been used to evaluate some aspects of cryopreserved organoids [4], comprehensive characterization of integrity and preservation of cellular composition of complex organoid tissues still needs further investigation.

Matrix-Assisted Laser Desorption Ionization (MALDI) Mass Spectrometry Imaging (MSI) is a label free technology that images hundreds of molecules across intact tissue sections, providing an overview of lipid and other metabolite distribution in samples while preserving their native tissue architecture. MALDI-MSI detects molecular ions separated by their mass-to-charge (m/z) ratio and it can achieve cellular resolution with pixel sizes of $5 \times 5\ \mu m^2$ [9]. This analysis could therefore provide more in depth information on tissue composition compared to immunofluorescence analysis. Specifically, MALDI-MSI can detect lipidomic signatures reflective of cellular specialization and maturation. Here we propose to apply this advanced MALDI-MSI to serve as assessment to verify and validate cell identity of the KOR product, including after cryopreservation and thawing, to support future scale up of organoid manufacture.

Materials and Methods

hiPSC maintenance

LUMC0072iCTRL01 (LUMC0072) were reprogrammed by LUMC hiPSC Hotel using RNA (detailed information at Human Pluripotent Stem Cell Registry, https://hpscreg.eu/) and cultured in Essential 8 medium (E8, Thermo Fisher Scientific) on vitronectin (Thermo Fisher Scientific) coated plates. Cells were passaged twice a week using UltraPure EDTA (Thermo Fisher Scientific). For differentiation, cells were dissociated as single cells using TrypLE Select (Thermo Fisher Scientific) and seeded at a density of 10,000 cells/cm^2. Medium was supplemented with RevitaCell (Thermo Fisher Scientific) for 24 h.

Kidney organoid differentiation

Differentiation of organoids was performed according to previously published protocols [10,11]. Briefly, differentiation was initiated on day 0 by incubating iPSCs in 8 µM CHIR99021 (R&D Systems) in STEMdiff APEL-2 medium (APEL-2) containing 1 % PFHMII (Protein-Free Hybridoma Medium-II, Life Technologies) and 1 % Antibiotic–Antimycotic (Life Technologies) (day 0). On day 4, APEL medium was supplementation with 200 ng/mL rhFGF9 (recombinant human Fibroblast growth factor-9, R&D Systems) and 1 µg/mL heparin (Sigma-Aldrich). On day 7 of differentiation the monolayer was pulsed for 1 h with 5 µM CHIR99021 in APEL before dissociation with Trypsin-EDTA. Cells were collected and assessed for cell viability and counted on an automated cell counter (NC-200). A total of 5 × 105 cells were centrifuged and transferred as cell clump onto a 0.4 µm pore polyester transwell membrane. On day 7 + 5, cytokines were withdrawn from the APEL medium, and organoid culture continued up to day 7 + 18.

Cryopreservation of iPSC-derived kidney progenitor cells and continued kidney organoid differentiation

For cryopreservation, iPSC-derived kidney progenitor cells were differentiated as described above and by Wiersma et al [4]. On day 7, after 1 h CHIR99021 pulse, cells were dissociated using Trypsin-EDTA for 5 min. After centrifugation, cells were resuspended in Nutrifreez (Biological Industries) and aliquoted in 8 × 106 cells/mL per vial (Biobanking and Cell Culture Cryogenic Tubes, Nunc). Vials were rate controlled frozen (− 1 °C/min in Mr. Frosty Freezing Containers) at − 80 °C for 24 h before transfer to the liquid nitrogen storage [4]. Progenitor cells were thawed after 1 – 15 weeks to resume kidney organoid differentiation. Cells were washed and resuspended in DMEM (Dulbecco's Modified Eagle Medium, Gibco) containing 10 % fetal bovine serum (Gibco) before assessing cell number and viability. Cell clumps containing 5 × 105 cells were centrifuged and placed on a transwell membrane. Experiments were conducted using three independent differentiations, with cells thawed three times from differentiation 1 and once each from differentiations 2 and 3.

Immunofluorescence analysis

Day 7 + 18 organoids were fixed in 2 % paraformaldehyde (PFA) for 20 min at 4 °C, and washed three times with phosphate-buffered saline (PBS) before storage at 4 °C. For immunofluorescence staining the organoids were set in agarose before embedding in paraffin and were then sectioned with a microtome at 5 µm. For antigen retrieval, slides were deparaffinated, rehydrated, and incubated in a pressure cooker in Tris-EDTA (pH9). Samples were then blocked with 10 % Donkey Serum (Sigma-Aldrich) and permeabilized with 0.3 % TritonX (Sigma-Aldrich) in PBS for 2 h at room temperature. Tissues slides were incubated with primary antibodies against Podocalyxin (R&D, AF1658), E-cadherin (BD, 61081), Lotus Tetragonolobus Lectin (LTL, Vector Laboratories, B-1325), Cubilin (Thermo Fisher Scientific, PA-83684 & Abcam, ab191073), SLC12A1 (Solute Carrier Family 12 Member 1, Invitrogen, PA5-80003), and Ki-67 (DAKO, M7240) in blocking buffer for 24 – 72 h at 4 °C. After three washes, sections were incubated for 2 h at room temperature with secondaries antibody donkey anti goat 488 (A-11055), donkey anti mouse 647 (A-31571), donkey anti rabbit 568 (A-10042), donkey anti rabbit 647 (A-31573), and streptavidin 532 (S-11224)(all Invitrogen). Samples were washed and nuclei were counterstained with Hoechst 33258, before embedding in Prolong Gold. White Light Laser Confocal Microscope TCS SP8 (Leica) with LAS-X 3.5.7 with LAS-X Image with 3D module were used to image all immunofluorescence samples.

Matrix-Assisted Laser Desorption Ionization (MALDI) Mass Spectrometry Imaging (MSI)

Tissue Preparation and Matrix Deposition. KOR and cryopreserved KOR (cKOR) derived from three independent differentiations (2 organoids per measurement; differentiation 1 contained 3 organoids), were snap frozen using liquid nitrogen and stored at -80 °C. Samples were embedded in 10 % gelatin and 10 µm cryosections were obtained at -20 °C using a Cryostar NX70 cryostat (Thermo Fisher Scientific). Sections were thaw-mounted onto indium-tin-oxide (ITO)-coated glass slides (VisionTek Systems Ltd) and subsequently dried in in a vacuum freeze-dryer for 15 min prior to matrix application. After the slides were dried, a 7 mg/mL MALDI-matrix solution (N-(1-naphthyl) ethylenediamine dihydrochloride (Sigma-Aldrich)) in a mixture of methanol/acetonitrile/deionized water (70, 25, 5 % v/v/v)) was applied using a SunCollect sprayer (SunChrom GmbH). Matrix deposition was performed in 21 sequential layers with gradually increasing flow rates: layer 1 – 3 at 5 µL/min, layer 4 – 6 at 10 µL/min, layer 7 – 9 at 15 µL/min and 10 – 21 at 20 µL/min (speed x, medium 1; speed y, medium 1; z position, 35).

MALDI-MSI measurement. MSI was performed using a RapifleX MALDI-TOF/TOF system (Bruker Daltonics GmbH). The instrument was calibrated with red phosphorus prior to data collection. Negative ion-mode mass spectra were acquired at a spatial resolution of 5 × 5 μm^2 over a mass range of m/z 80 – 1000 in reflection mode. Each pixel was sampled with 15 laser shots at laser repetition rate of 10 kHz. Data acquisition and initial visualization was

performed using flexControl (Version 4.0, Bruker Daltonics) and flexImaging 5.0 (Bruker Daltonics). Samples on the same slide were measured in randomized order.

Immunofluorescence staining after MALDI-MSI. Following MALDI-MSI data acquisition, excess matrix was removed by sequential washes in 100 % ethanol (2 × 5 min), 75 % ethanol (1 × 5 min) and 50 % ethanol (1 × 5 min). Organoid sections were fixed with 4 % PFA for 10 min and blocked with 3 % normal goat serum, 2 % bovine serum albumin and 0.01 % Triton X-100-X100 in PBS for 1 h at room temperature. Primary antibodies against E-cadherin (BD Biosciences, 610181), Nephrin (R&D, AF4269) and LTL (Vector Laboratories, B-1325) were incubated overnight at 4°C. Corresponding fluorescent-labelled secondary antibodies (donkey anti mouse 488 (A21202), donkey anti sheep 647 (A21448), and streptavidin 532 (S-11224)(all Invitrogen) were incubated for 1 h at room temperature. Sections were embedded in ProlongTM gold antifade mountant (Invitrogen, P36930) and imaged using 3D Histech Pannoramic MIDI Scanner (Sysmex).

MSI data processing and analysis. Raw MALDI-MSI data were imported in SCiLS Lab 2016b (SciLS, Bruker Daltonics) and baseline corrected using convolution algorithm. Spectra were normalized to total ion count (TIC) and peaks were selected with a signal-to-noise-ratio > 3. Features with m/z > 400 that were not associated with matrix peaks (predominately phospholipids) were extracted. Peak intensities for all measured pixels of the selected features were exported and used for downstream analysis. For uniform manifold approximation and projection (UMAP) analysis, TIC-normalized intensities were scaled by 100 and converted to integers to create a count matrix. The resulting matrices were normalized and scaled using SCTransform to generate a 2-dimensional UMAP map using Seurat [12] in R (version 4.0). Data from different differentiations were integrated with batch correction in Seurat. Cluster locations on tissue sections were aligned to the immunofluorescence staining, and cell types were identified based on both marker expression and morphology. The differential abundance of lipids between clusters was analyzed using FindAllMarkers function in Seurat.

Molecular histology. The integrated datasets were used to generate 3-dimensional UMAP representations with Seurat and plotly. The UMAP embedding coordinates were mapped to RGB color channels and together with pixel coordinates exported from SCiLS Lab, a M x N x 3 matrix was created for visualization in Matlab R2019a. 3D scatter plots of the UMAP image were generated in Matlab to illustrate spatial lipidomic patterns across organoid sections.

Results

Kidney organoids preserved capacity to differentiate after cryopreservation at day 7 progenitor stage

iPSC-derived kidney organoid progenitors at day 7 of differentiation were either cultured in vitro for the duration of the experiment (KOR) or cryopreserved at -190 °C for periods ranging from 1 and 15 weeks before thawing (Figure 1A). Three independent differentiations, with KOR and cKOR in each differentiation, were cultured until organoids reached day 7 + 18. Post thaw viability of the day 7 cryopreserved progenitor cell population was >94 %, comparable to that in KOR on day 7 (Figure 1B), indicating efficient recovery and suggesting that the cryopreservation procedure (such as medium and dissociation reagent, and thawing time) did not adversely affect cell survival. Formed organoids were assessed using brightfield imaging and demonstrated a high degree of morphological similarity between the organoids (Figure 1C, Supplemental Figure 1A). Three nephron segments were further identified in both KOR and cKOR using kidney-specific markers: Podocalyxin (glomerular structures), Cubilin (proximal tubules) and E-cadherin (distal tubules). Immunofluorescence overview images confirmed that these nephron structures were present in all organoids (Figure 1C and Supplemental Figure 1A). In both KOR and cKOR, presence of Loop of Henle (SLC12A1), proximal tubules (LTL), and proliferating cells (Ki-67) was observed (Figure 1D-E, Supplemental Figure 1B-C, and Supplemental Figure 2).

Molecular and lipid heterogeneity characterized by spatial lipidomics in KOR and cKOR

Next, we aimed to perform a more in depth characterization of all KORs and cKORs. We applied high-spatial-resolution MALDI-MSI to evaluate the spatial lipid profile at single cell resolution (5 × 5 μm^2 pixel size). The UMAP-plot visualized distinct populations in organoids (KOR and cKOR combined) based on their lipid profile expression allowing us to identify 10 different cell types (Supplemental Figure 3A). Following MALDI-MSI analysis, the same tissue slides were stained to identify nephron segments using markers for: glomeruli (Nephrin), proximal tubule (LTL) and distal tubule (E-cadherin), and imaged using multiplexed immunofluorescence microscopy. These immunofluorescence microscopy images, highlighting 3 nephron structures, were aligned with the MALDI-MSI data. This combined analysis allowed for unbiased molecular identification of the lipid based population in kidney organoids, revealing 10 distinct cell types (Figure 2A and Supplemental Figure 3B) and assisted in discriminating multiple specialized cell types that were not classified using immunofluorescence analysis only. Specific cell populations were assigned based on their most characteristic phospholipids (Supplemental Figure 3B) and example images illustrate the spatial distribution of individual lipids (m/z) throughout the organoid (Supplemental Figure 3C).

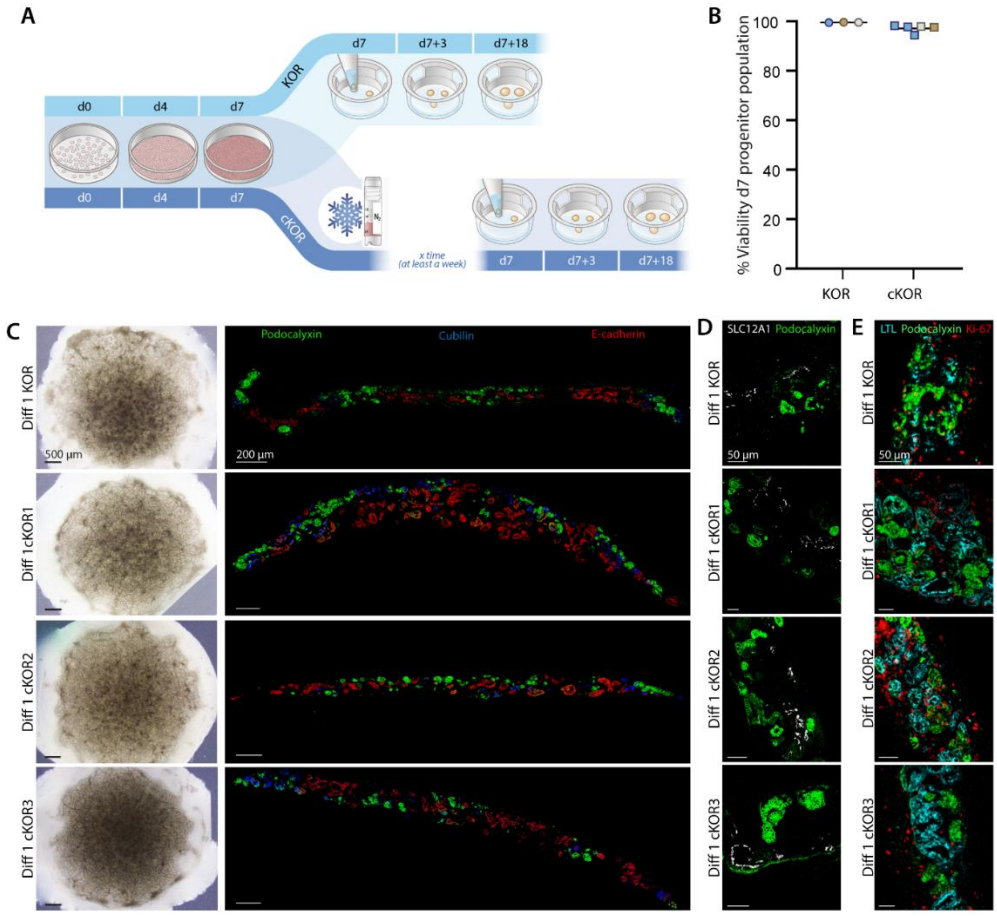

Figure 1. Similarity between kidney organoids (KOR) and organoids from cryopreserved progenitors (cKOR) based on brightfield and immunofluorescence analysis

A. *A. Graphical overview for the generation of kidney organoids (KOR) and organoids upon cryopreservation (cKOR) as progenitors on day 7. Time between cryopreservation and thawing was between 1 – 15 weeks.* ***B.*** *Cell viability was measured on d7 of differentiation for KOR and cKOR just after thawing. Dots/squares represent the percentage of viability per differentiation and mean is displayed as a line. Each color corresponds to an independent experiment* ***C.*** *Brightfield images and immunofluorescence overview of sections of KOR and cKOR (cKOR1, cKOR2, cKOR3) within differentiation 1 display comparable kidney organoid morphology. Immunofluorescence overview images show distribution of Podocalyxin (glomerular structures), Cubilin (proximal tubule) and E-cadherin (distal tubule).* ***D.*** *Magnified immunofluorescence images of KOR and cKOR (cKOR1, cKOR2, cKOR3) highlighting SLC12A1 (loop of Henle) and Podocalyxin (glomerular structures).* ***E.*** *Immunofluorescence images of KOR and cKOR (cKOR1, cKOR2, cKOR3) showing proliferation marker Ki-67, LTL (proximal tubule) and Podocalyxin (glomerular structures).*

Subsequently, we compared lipid profiles between KOR and cKOR. UMAP analysis showed that both KOR (7 organoids in total) and cKOR (10 organoids in total) from 3 independent differentiation experiments contain the same cell populations (Figure 2B). A total of 10 cell types, including podocyte, proximal tubule and distal tubule were identified in both KOR and cKOR, and the lipid profiles were highly consistent across the 3 independent

differentiations (Figure 2C-E). Populations were characterized based on lipid profiles and immunofluorescence analysis of nephron structures (Figure 2A). Within distal tubules stained for E-cadherin, two distinct populations were identified based on their lipid profile (distal 1 & 2). These two populations likely represent different stages of distal tubule maturation, as suggested by developing kidney cell classifier [13]. In the population designated as developing tubule, overlap with proximal (LTL) and distal (E-cadherin) tubule markers was observed. The epithelial mixture population was positive for both proximal (LTL) and glomerular (Nephrin) markers. The four remaining populations could represent stromal cells (stromal 1-4), as they lacked nephron-associated characteristics and correspond to populations in kidney organoid as defined by DevKidCC [13]. The distribution of population clusters from all experiments are displayed in Figure 2F. Within each differentiation experiment, KOR and cKOR distributions are comparable, although differences can be observed between differentiation experiments. For example, a large podocyte population in differentiation 2 is very evident in both KOR and cKOR compared to differentiation 1 and 3, and a similar pattern was observed for the epithelial mixture population in differentiation 3. Other populations in kidney organoids displayed consistent distributions of within a given differentiation experiment but showed slightly more variability across different experiments.

MALDI-MSI can be used as a tool for phenotypic characterization iPSC-kidney organoids

Before stem cell-derived tissues can be utilized as a clinical product, they must undergo quality assessment and phenotypic characterization. This applies to iPSCs themselves as well as for their differentiated derivatives. Given the potential variability of differentiations after freeze-thaw, it is important to define release criteria for such cell products. We propose that post-thaw viability of renal progenitors should exceed 90 % to ensure the generation of viable kidney organoids. Secondly, the presence and spatial distribution of renal cell populations in iPSC-derived renal organoids should be evaluated. We analyzed the proportion of each population in individually measured KOR and cKOR (Figure 3) and observed a high degree of similarity between renal cell populations in KOR and cKOR. The majority of populations overlapped except for proximal tubules in cKOR, where a higher proportion of proximal tubular cells was detected compared to KOR.

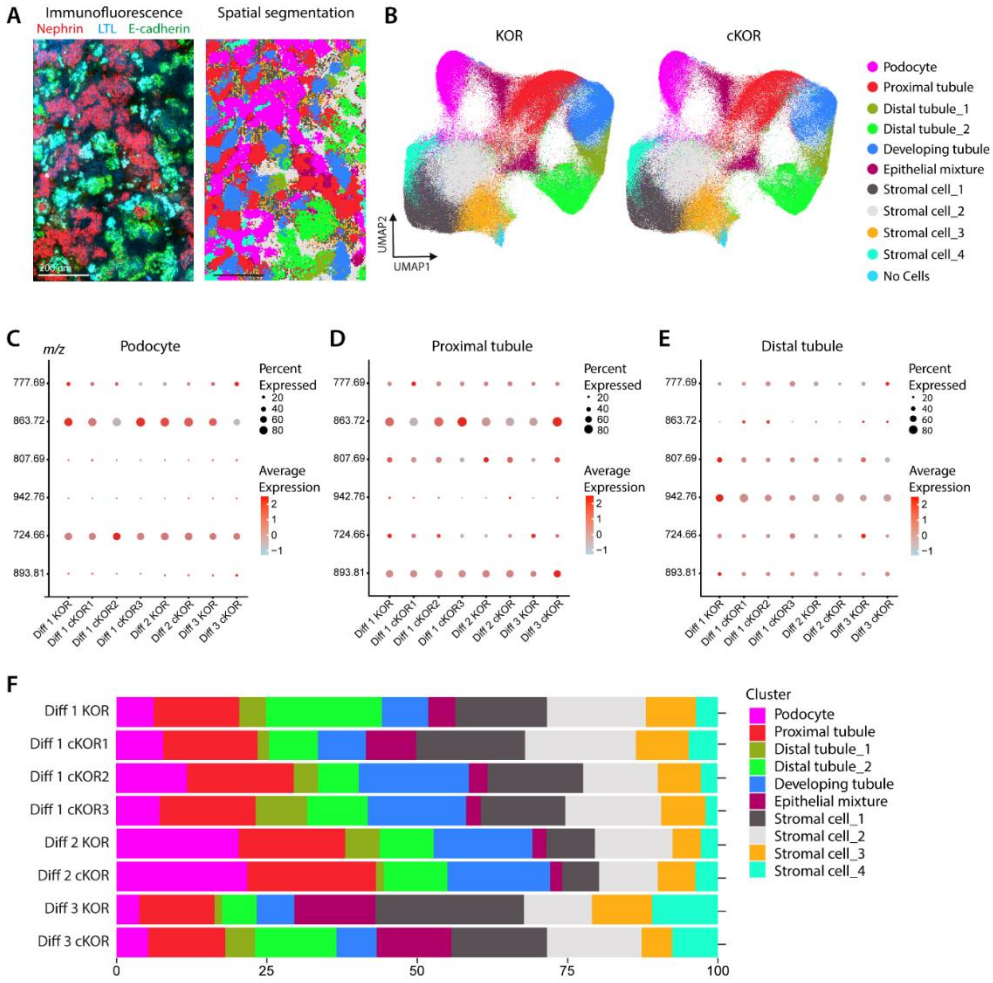

Figure 2. Lipidomic characterization and comparison of kidney organoids (KOR) and organoids from cryopreserved progenitors (cKOR)

A. *Post-MALDI-MSI immunofluorescence staining (left) for Nephrin (glomerulus), LTL (proximal tubule) and E-cadherin (distal tubule), and spatial segmentation (right) by micrograph of cell-type-specific lipid species distribution as recorded by MALDI-MSI at 5 × 5 µm² pixel size showing lipid heterogeneity between cell populations in KOR.* ***B.*** *Uniform manifold approximation and projection (UMAP) plot comparing lipid profiles from KOR and cKOR of MALDI-MSI data. 10 populations including nephron and stromal cell types are displayed.* ***C-E****. Dot plot showing the abundance of cluster-specific lipid features in different cell types from podocyte (****C****), proximal tubule (****D****) and distal tubule (****E****). The distal tubule population displayed in D is a combination of distal tubule 1 & 2 (shown in* ***A****).****F.*** *Comparison of the percentage of cell type composition between KOR and cKOR from 3 independent experiments (diff 1, 2 and 3) where 3 independently thawed organoids were compared for differentiation 1 (cKOR1, -2 and -3), and 1 cKOR for differentiation 2 and 3.*

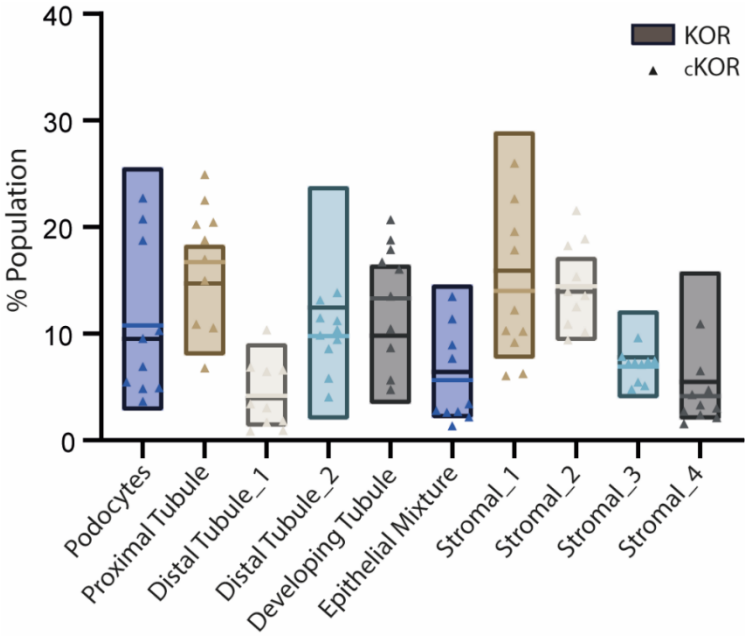

Figure 3. Phenotypic assessment of kidney organoids (KOR) and from cryopreserved progenitors (cKOR) shows comparable population distribution

Overview and overlay of percentages of each individual population found in the KOR and cKOR from MALDI-MSI data. The bars in the plot indicate percentage of populations from KOR, while the triangles represent the percentages of individually measured populations of cKOR. The mean is displayed as a line.

Discussion

Organoids hold great potential in regenerative medicine, with kidney organoid technology contributing significantly to this progress. Key advancements include the transition from 2D to 3D culture, scale-up and scale out of differentiation products and improving cryopreservation techniques. Thorough qualitative assessment and establishment of release criteria are essential for application of these tissues as clinical product. Here we highlight MALDI-MSI as a tool for in depth characterization of cellular composition of kidney organoids while preserving tissue architecture.

To reduce the need for continues and long term stem cell and kidney organoid culture, we cryopreserved kidney organoid progenitors at day 7 of differentiation [4]. We used a GMP-compliant cryopreservation medium that has successfully been applied in other protocols for preserving pluripotent stem cells and their differentiated derivatives [14-16]. Recent studies, such as Mashouf et al. explored an alternative approach, applying cryopreservation of whole kidney organoids through slow freezing and vitrification [17]. While whole-organoid cryopreservation may impact structural integrity and function of kidney organoids, Mashouf et al. demonstrate preservation of organoid size, viability, and nephron structures. These findings supports the concept of a biobank for ready-to-use organoids or progenitors.

Maintaining high cell viability before and after cryopreservation is crucial for generating functional tissues capable of forming nephron structures. Such quality guidelines have also been suggested for chimeric antigen receptor (CAR) and T-cell receptor (TCR) T-cells where the cell viability needs to exceed 50 % and post-thaw marker expression had to remain within ~20 % of pre-cryopreservation levels [18]. Our post-thaw viability is comparable or higher to other iPSC-derived cells types, such as cardiomyocytes (~96 %) [19] or dopaminergic neurospheres (± 63 %) [20].

Minimizing batch-to-batch variability is equally crucial for reproducibility, reliability, and scalability. hiPSC-derived kidney organoids are complex tissues, with nephron maturation, patterning, and both on- and off-target differentiation contributing significantly to variability between batches [21]. Our kidney organoids developed from cryopreserved progenitors exhibited structural consistency, as demonstrated through both conventional brightfield microscopy and immunofluorescence imaging, demonstrating presence of nephron structures as well as active proliferation.

Unfortunately, conventional immunofluorescence analysis is limited by the number of predefined markers that can be used simultaneously, typically restricted to around five (due to signal overlap in secondary label detection and host species limitations). As a result,

multiple tissue sections or whole organoids are often required for a comprehensive overview of all cell populations. Compared with conventional approaches such as immunofluorescence staining or H&E staining, MALDI-MSI enables quality assessment of kidney organoids through unsupervised analysis of hundreds of lipids, thereby providing a more precise reflection of cellular states. For example, in our previous work, we demonstrated that spatial lipid distributions can be used to distinguish developmental states across different regions of organoids[22], as well as to identify areas of injury during kidney perfusion [23]. Although our current study did not evaluate injury-associated lipid markers in kidney organoids, MALDI-MSI could in the future provide a promising platform for investigations of cellular stress, metabolic changes, or injury responses. Nonetheless, MALDI-MSI is limited by spatial resolution compared with staining-based analyses, which is performed at 5 μm and may fail to capture certain finer details.

High spatial resolution MALDI-MSI offers a complementary approach for characterizing organoids. This approach is non-destructive and label-free, preserving tissue architecture while enabling simultaneous detection of hundreds of metabolites and lipids at single cell resolution. It allows for unbiased molecular histology of a wide range of metabolites and biomolecules simultaneously. This allows identification of cell-type-specific metabolic or lipidomic heterogeneity, that may not be captured by conventional immunofluorescence. This assists in detailed evaluation of tissue architecture and cellular microenvironments and subtle cell-type specific variations (such as diseased or immature areas during kidney organoid development), which is particularly valuable in complex tissues such as kidney organoids [9,22].

In this study, we validated cKOR and demonstrated the utility of MALDI-MSI for phenotypic characterization and qualitative assessment. Cryopreserved progenitors maintained high post-thaw viability and generated KORs containing all nephron cell populations. Their lipid profiles were comparable to non-cryopreserved KORs, providing a comprehensive evaluation of cellular composition. MALDI-MSI therefore offers a powerful platform for single-cell-level analysis while preserving spatial architecture, with potential applications for qualitative screening of cryopreserved kidney organoids prior to clinical use, as well as in disease modeling and developmental biology.

Acknowledgements

This work is supported by the Novo Nordisk Foundation Center for Stem Cell Medicine (reNEW, supported by Novo Nordisk Foundation grant (NNF21CC0073729)) (CvdB, TR). We thank Christian Freund (hiPSC core facility, LUMC, Leiden, the Netherlands) for providing hiPSC line LUMC0072iCTRL01. We acknowledge the support of Manon Zuurmond (LUMC, Leiden, the Netherlands). We thank the Light and Electron Microscopy Facility and the Center for Proteomics and Metabolomics (LUMC, Leiden, the Netherlands) for assistance and maintenance of the equipment.

References

1 Khoshdel-Rad N., Ahmadi A., Moghadasali R. Kidney organoids: current knowledge and future directions. Cell Tissue Res 2022;387(2):207-224, doi:https://doi.org/10.1007/s00441-021-03565-x.

2 Koning M., van den Berg C.W., Rabelink T.J. Stem cell-derived kidney organoids: engineering the vasculature. Cell Mol Life Sci 2020;77(12):2257-2273, doi:https://doi.org/10.1007/s00018-019-03401-0.

3 Chambers B.E., Weaver N.E., Wingert R.A. The "3Ds" of Growing Kidney Organoids: Advances in Nephron Development, Disease Modeling, and Drug Screening. Cells 2023;12(4) doi:https://doi.org/10.3390/cells12040549.

4 Wiersma L.E., Avramut M.C., Lievers E. et al. Large-scale engineering of hiPSC-derived nephron sheets and cryopreservation of their progenitors. Stem Cell Res Ther 2022;13(1):208, doi:https://doi.org/10.1186/s13287-022-02881-5.

5 Lawlor K.T., Vanslambrouck J.M., Higgins J.W. et al. Cellular extrusion bioprinting improves kidney organoid reproducibility and conformation. Nat Mater 2021;20(2):260-271, doi:https://doi.org/10.1038/s41563-020-00853-9.

6 Kumar S.V., Er P.X., Lawlor K.T. et al. Kidney micro-organoids in suspension culture as a scalable source of human pluripotent stem cell-derived kidney cells. Development 2019;146(5) doi:https://doi.org/10.1242/dev.172361.

7 Przepiorski A., Crunk A.E., Holm T.M. et al. A Simplified Method for Generating Kidney Organoids from Human Pluripotent Stem Cells. J Vis Exp 2021(170) doi:https://doi.org/10.3791/62452.

8 Novoa J.J., Westra I.M., Steeneveld E. et al. Good Manufacturing Practice-compliant human induced pluripotent stem cells: from bench to putative clinical products. Cytotherapy 2024;26(6):556-566, doi:https://doi.org/10.1016/j.jcyt.2024.02.021.

9 Wang G., Heijs B., Kostidis S. et al. Analyzing cell-type-specific dynamics of metabolism in kidney repair. Nat Metab 2022;4(9):1109-1118, doi:https://doi.org/10.1038/s42255-022-00615-8.

10 Takasato M., Er P.X., Chiu H.S. et al. Kidney organoids from human iPS cells contain multiple lineages and model human nephrogenesis. Nature 2016;536(7615):238, doi:https://doi.org/10.1038/nature17982.

11 van den Berg C.W., Ritsma L., Avramut M.C. et al. Renal Subcapsular Transplantation of PSC-Derived Kidney Organoids Induces Neo-vasculogenesis and Significant Glomerular and Tubular Maturation In Vivo. Stem Cell Rep 2018;10(3):751-765, doi:https://doi.org/10.1016/j.stemcr.2018.01.041.

12 Stuart T., Butler A., Hoffman P. et al. Comprehensive Integration of Single-Cell Data. Cell 2019;177(7):1888-1902 e1821, doi:https://doi.org/10.1016/j.cell.2019.05.031.

13 Wilson S.B., Howden S.E., Vanslambrouck J.M. et al. DevKidCC allows for robust classification and direct comparisons of kidney organoid datasets. Genome Med 2022;14(1):19, doi:https://doi.org/10.1186/s13073-022-01023-z.

14 Breunig M., Merkle J., Melzer M.K. et al. Differentiation of human pluripotent stem cells into pancreatic duct-like organoids. STAR Protoc 2021;2(4):100913, doi:https://doi.org/10.1016/j.xpro.2021.100913.

15 Reichman S., Slembrouck A., Gagliardi G. et al. Generation of Storable Retinal Organoids and Retinal Pigmented Epithelium from Adherent Human iPS Cells in Xeno-Free and Feeder-Free Conditions. Stem Cells 2017;35(5):1176-1188, doi:https://doi.org/10.1002/stem.2586.

16 Kuznitsov-Yanovsky L., Mayshar Y., Ben-Yosef D. Modeling FXS: Human Pluripotent Stem Cells and In Vitro Neural Differentiation. Methods Mol Biol 2019;1942:89-100, doi:https://doi.org/10.1007/978-1-4939-9080-1_8.

17 Mashouf P., Tabibzadeh N., Kuraoka S. et al. Cryopreservation of human kidney organoids. Cell Mol Life Sci 2024;81(1):306, doi:https://doi.org/10.1007/s00018-024-05352-7.

18 Cai Y., Prochazkova M., Jiang C. et al. Establishment and validation of in-house cryopreserved CAR/TCR-T cell flow cytometry quality control. J Transl Med 2021;19(1):523, doi:https://doi.org/10.1186/s12967-021-03193-7.

19 van den Brink L., Brandao K.O., Yiangou L. et al. Cryopreservation of human pluripotent stem cell-derived cardiomyocytes is not detrimental to their molecular and functional properties. Stem Cell Res 2020;43:101698, doi:https://doi.org/10.1016/j.scr.2019.101698.

20 Hiramatsu S., Morizane A., Kikuchi T. et al. Cryopreservation of Induced Pluripotent Stem Cell-Derived Dopaminergic Neurospheres for Clinical Application. J Parkinsons Dis 2022;12(3):871-884, doi:https://doi.org/10.3233/JPD-212934.

21 Phipson B., Er P.X., Combes A.N. et al. Evaluation of variability in human kidney organoids. Nat Methods 2019;16(1):79-87, doi:https://doi.org/10.1038/s41592-018-0253-2.

22 Wang G., Heijs B., Kostidis S. et al. Spatial dynamic metabolomics identifies metabolic cell fate trajectories in human kidney differentiation. Cell Stem Cell 2022;29(11):1580-1593 e1587, doi:https://doi.org/10.1016/j.stem.2022.10.008.

23 de Haan M.J.A., Jacobs M.E., Witjas F.M.R. et al. A cell-free nutrient-supplemented perfusate allows four-day ex vivo metabolic preservation of human kidneys. Nat Commun 2024;15(1):3818, doi:https://doi.org/10.1038/s41467-024-47106-w.

Supplemental Figures

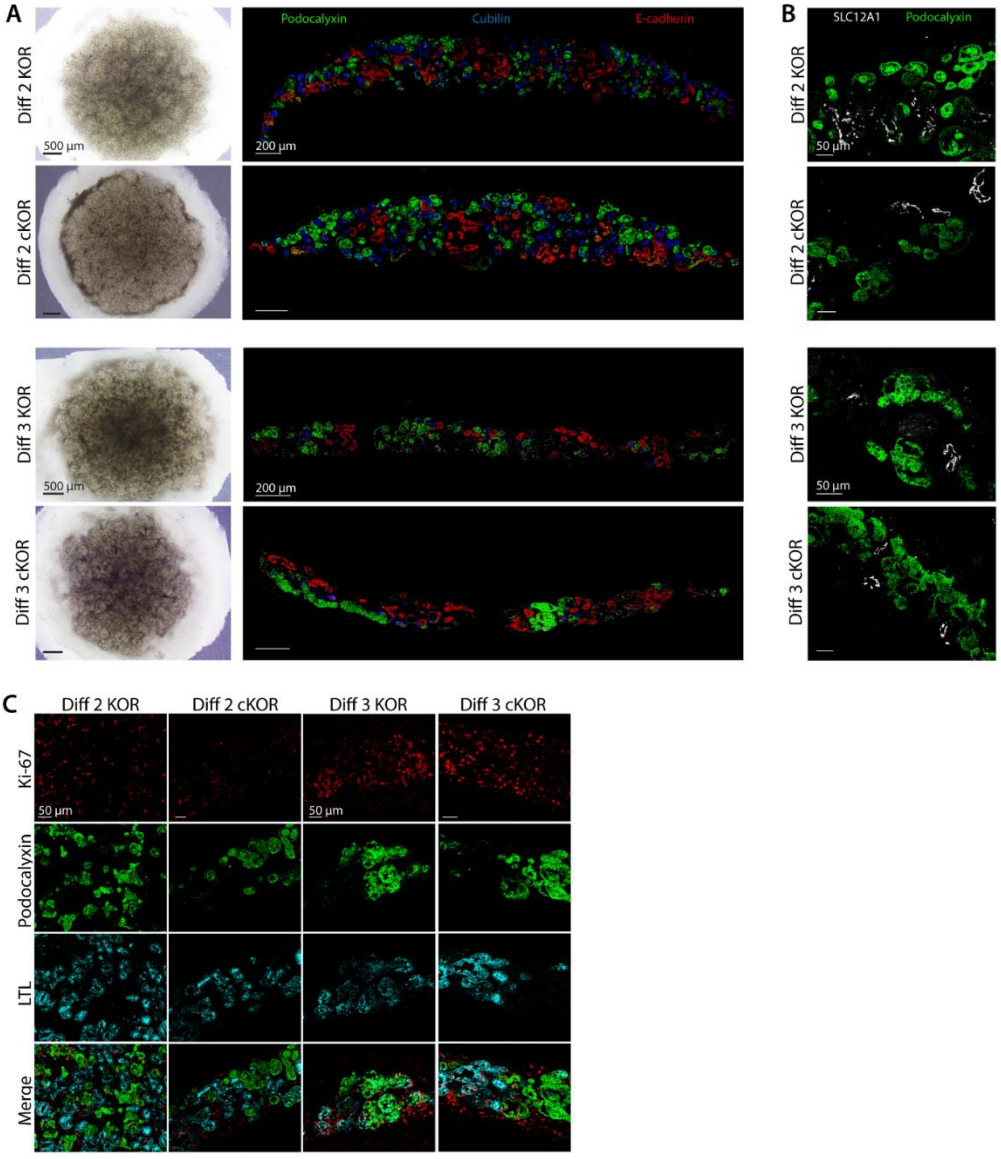

Supplemental Figure 1. Similarity between kidney organoids (KOR) and organoids from cryopreserved progenitors (cKOR) in differentiation experiment 2 and 3

A. *Brightfield images and immunofluorescence overview of KOR and cKOR from differentiation 2 and 3 showing similar morphology of KOR and cKOR within and between both differentiations and equal distribution of Podocalyxin (glomerular structures), Cubilin (proximal tubule) and E-cadherin (distal tubule).* ***B.*** *Magnified immunofluorescence images with KOR and cKOR highlighting SLC12A1 (loop of Henle) and Podocalyxin (glomerular structure).* ***C.*** *Immunofluorescence images with KOR and cKOR showing proliferation (Ki-67), and distribution of LTL (proximal tubule) and SLC12A1 (distal tubule).*

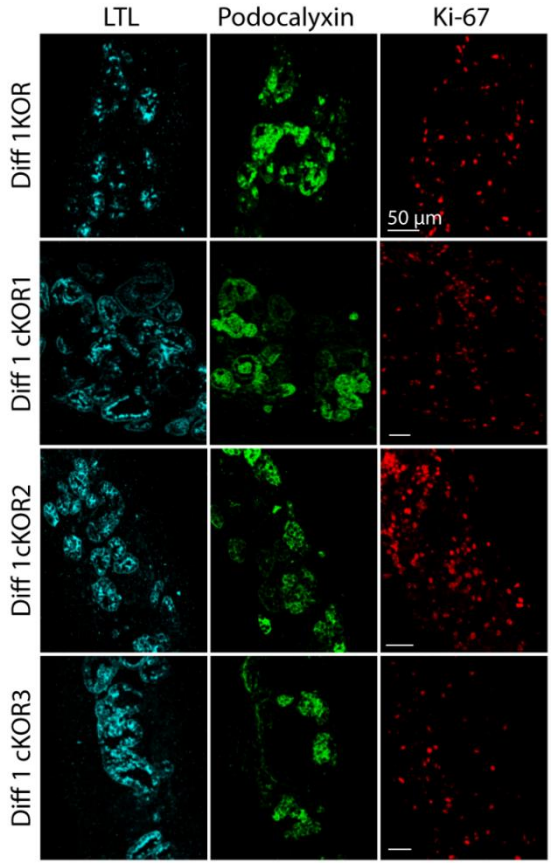

Supplemental Figure 2. Visualization of kidney organoids (KOR) and organoids from cryopreserved progenitors (cKOR)

Single immunofluorescence images (matching merged in Figure 1E) of differentiation 1 with KOR and cKOR showing proliferation (Ki-67), and distribution of LTL (proximal tubule) and SLC12A1 (distal tubule).

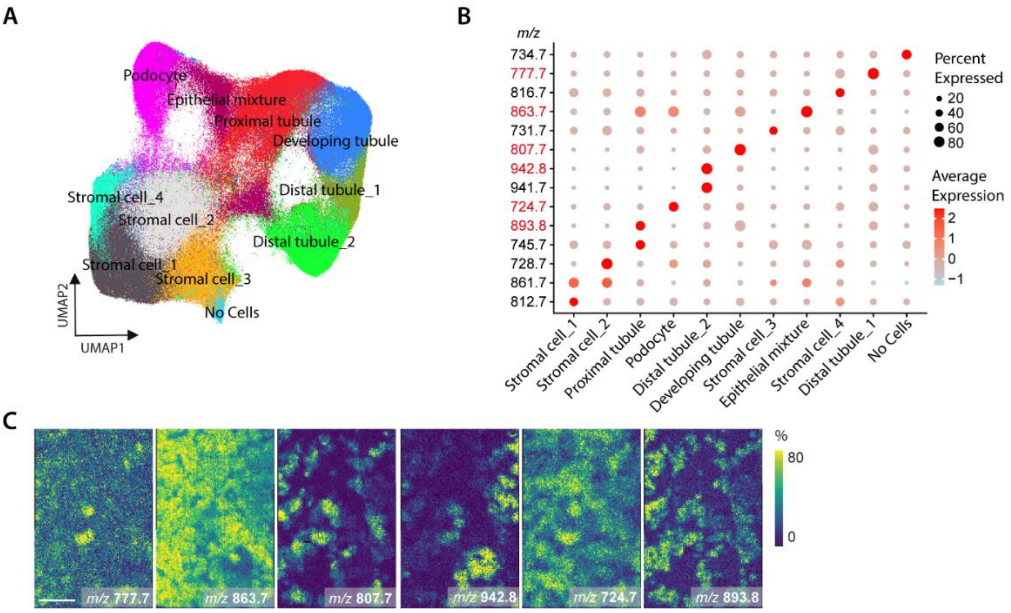

Supplemental Figure 3. Setup to study lipid heterogeneity in kidney organoids

A. *Uniform manifold approximation and projection (UMAP) plot visualizing lipid heterogeneity in kidney organoids from different conditions (7 kidney organoids (KOR) and 10 generated from cryopreserved progenitors (cKOR) combined) allows for identification of the main epithelial cell types, visualized in UMAP plot of 180 lipid m/z features from MALDI-MSI data (5 x 5 µm² pixel size).* ***B.*** *Dot plots display expression of cluster-specific lipid features. Red text highlights selected lipids in* ***C****.* ***C.*** *Micrograph of cell-type-specific lipid species distribution as recorded by MALDI-MSI at 5 × 5 µm² pixel size. Spatial distribution of cluster-specific lipid features as labeled red in* ***B****.*